Carbon 162 (2020) 1–12

Contents lists available at ScienceDirect

Carbon

journal homepage: www.elsevier.com/locate/carbon

Influence of diamond crystal orientation on the interaction with biological matter

Viraj Damle [a, 1], Kaiqi Wu [a, 1], Oreste De Luca [b], Natalia Ortí-Casañ [c], Neda Norouzi [a], Aryan Morita [a, d], Joop de Vries [a], Hans Kaper [a], Inge S. Zuhorn [a], Ulrich Eisel [c], Danny E.P. Vanpoucke [e, f], Petra Rudolf [b], Romana Schirhagl [a, *]

[a] University of Groningen, University Medical Center Groningen, Antonius Deusinglaan 1, 9713AV, Groningen, the Netherlands
[b] Zernike Institute for Advanced Materials, Nijenborgh 4, 9747 AG, Groningen, the Netherlands
[c] Department of Molecular Neurobiology, Groningen Institute for Evolutionary Life Sciences, Faculty of Science and Engineering, University of Groningen, Nijenborgh 7, 9747 AG, Groningen, the Netherlands
[d] Department of Dental Biomedical Sciences, Faculty of Dentistry, Universitas Gadjah Mada, Jalan Denta 1, Yogyakarta, 55281, Indonesia
[e] Institute for Materials Research (IMO), Hasselt University, 3590, Diepenbeek, Belgium
[f] IMOMEC, IMEC vzw, 3590, Diepenbeek, Belgium

ARTICLE INFO

Article history:
Received 19 September 2019
Received in revised form
30 January 2020
Accepted 31 January 2020
Available online 7 February 2020

ABSTRACT

Diamond has been a popular material for a variety of biological applications due to its favorable chemical, optical, mechanical and biocompatible properties. While the lattice orientation of crystalline material is known to alter the interaction between solids and biological materials, the effect of diamond's crystal orientation on biological applications is completely unknown. Here, we experimentally evaluate the influence of the crystal orientation by investigating the interaction between the <100>, <110> and <111> surfaces of the single crystal diamond with biomolecules, cell culture medium, mammalian cells and bacteria. We show that the crystal orientation significantly alters these biological interactions. Most surprising is the two orders of magnitude difference in the number of bacteria adhering on <111> surface compared to <100> surface when both the surfaces were maintained under the same condition. We also observe differences in how small biomolecules attach to the surfaces. Neurons or HeLa cells on the other hand do not have clear preferences for either of the surfaces. To explain the observed differences, we theoretically estimated the surface charge for these three low index diamond surfaces and followed by the surface composition analysis using x-ray photoelectron spectroscopy (XPS). We conclude that the differences in negative surface charge, atomic composition and functional groups of the different surface orientations lead to significant variations in how the single crystal diamond surface interacts with the studied biological entities.

1. Introduction

Diamond has been a popular material for a variety of biological applications due to its favorable chemical, optical, mechanical and biocompatible properties [1]. For instance, diamond coatings are used to improve cell adherence and proliferation in biomedical implants [2,3]. In neurobioscience [4], chemically patterned single crystal diamond and diamond thin films were investigated for promoting cell attachment [5,6] and neuronal growth [7], respectively. Many efforts have been focused on developing novel diamond coatings to make diamond films suitable for biological applications through repelling unwanted protein adsorption [8–12]. Nanocrystalline diamond films [13], diamond films having nanoscale needle-shape morphology [14] and boron-doped diamond [15] having a specific surface termination have also been investigated to reduce bacterial adhesion and biofouling. Similarly to bulk diamond and diamond coatings, fluorescent nanodiamonds (FNDs) have been explored for a variety of biological applications, as biomarkers [16], intracellular sensors [17–21] and drug delivery vehicles [22,23]. They are attractive for these applications due to their lack of cytotoxicity, modifiable surface chemistry [24] and

* Corresponding author. University of Groningen, University Medical Center Groningen, Antonius Deusinglaan 1, 9713AV, Groningen, the Netherlands.
E-mail address: romana.schirhagl@gmail.com (R. Schirhagl).
[1] contributed equally.

https://doi.org/10.1016/j.carbon.2020.01.115

photostable fluorescence [25]. Despite the wide range of biological applications, the effect of diamond's crystal orientation on these applications has not been investigated yet.

For other materials, crystal orientation has only seldomly been taken into account. It has been shown that crystal orientation can affect biological applications such as protein adsorption, cellular adhesion and proliferation or biofouling. In particular, Zhuang et al. demonstrated the preferential adsorption of negatively charged bovine serum albumin and positively charged lysosome protein on the different crystal planes of hydroxyapatite (HAp) crystals [26]. Similar protein adsorption studies have been conducted on calcium phosphate crystals [27]. In addition to protein adsorption, interaction of cells with different crystal planes of the HAp [28], titanium [29], calcite and calcium (R,R)-tartrate tetrahydrate crystals [30] have also been explored. Furthermore, different bioleaching rates for various surface orientations of pyrite crystals were observed [31].

The tetrahedral lattice of the diamond crystal gives rise to a variety of crystal orientations. Depending on the lattice plane, the number of carbon atoms per unit lattice changes and their bonding arrangement is different. This leads to the alteration in the surface functional groups and the overall surface reactivity. In fact, Wang and co-workers experimentally showed that the <001> plane of a diamond crystal has a higher coverage of carboxylic acid groups than the <111> surface [32]. Moreover, the difference in reactivity for different surface orientations has also been utilized to realize diverse surface topographies in single crystal diamond using reactive ion etching as the rate at which the reactive ions remove atoms depends on the surface orientations [33]. Here, we examined if the differences in surface structure of the three low index planes of a diamond crystal also affect biological applications.

To this end, we first characterized the surface roughness of these <100>, <110> and <111> diamond surfaces via atomic force microscopy (AFM). Next, we experimentally evaluated the influence of the surface orientation on the interaction with biomolecules, cell culture medium and bacteria. We show that all these interactions are greatly influenced by the crystal orientation of diamond. Furthermore, we investigated if adhesion and proliferation of mammalian cells, HeLa cells and primary neurons in particular, differ depending on the specific surface plane. Both cell types attached and grew on the diamond surfaces normally compared to the standard culture plates. However, there was no statistically significant difference observed between the three crystal orientations investigated. To explain the observed differences in interaction between biological matter and the three crystals, we theoretically estimated the surface charge for these three surfaces and analyzed the surface composition using x-ray photoelectron spectroscopy (XPS). These results show that there are indeed substantial differences in negative charge, atomic composition and abundance of functional groups between the three low index surfaces, which cause significant variations in how single crystal diamond interacts with biomolecules, cell culture medium, mammalian cells and bacteria.

2. Materials and methods

2.1. Diamond crystals and surface treatments

All the biological experiments in this work with minimum two repetitions per experiment were conducted on high pressure, high temperature (HPHT) single crystal diamonds with <100>, <110> and <111> surface orientations. The diamond plates were purchased from Almax easyLab (Belgium). All the diamond crystals were cleaned before every experiment using a well-established acid boiling protocol. Specifically, crystals were cleaned in a boiling mixture of sulphuric acid (Sigma-Aldrich, the Netherlands) and nitric acid (Merck, the Netherlands) mixed in the ratio of 1:3 at 140 °C for 4 h [32,34]. After boiling, the mixture was allowed to cool to the room temperature, then the diamonds were taken out, rinsed multiple times with MilliQ water and subsequently dried with lens cleaning tissue (Thorlabs, Germany). With this protocol, oxidized diamond surfaces were obtained. These surfaces were either directly used for the experiments or used for further surface modification. In particular, reduced, pristine and 1-(3-dimethylaminopropyl)-3-ethylcarbodiimide hydrochloride-N-hydroxysuccinimide (EDC-NHS) activated surfaces were fabricated from the oxidized diamond surfaces. The reduced diamond surfaces were obtained following the procedure described by Krüger et al. [35]. Specifically, the diamond plates were placed in a 10 mL two-necked flask under nitrogen. Then, 5 mL of 1 M $BH_3 \cdot THF$ in dry tetrahydrofurane (THF) (Sigma-Aldrich, Germany) was added and the reaction mixture was refluxed for 24 h. After cooling to room temperature, hydrolysis was carried out with 2 M hydrochloric acid until the hydrogen bubbling completely vanished. The HPHT diamond plates were washed two times with acetone and three times with MilliQ water, followed by drying with lens cleaning tissue. To fabricate the pristine diamond surface, acid cleaned surfaces were quickly transferred into XPS equipment where they were bombarded by argon ions.

2.2. Biomolecule conjugation

The cleaned <100>, <110>, and <111> diamond crystals were put in 35 mm Petri dish in which 2 mL of a freshly prepared EDC-NHS (50 mM each) solution made with cold MilliQ water [36,37]. Plates were incubated for 2 h at room temperature to activate the carboxyl groups on the diamond surface. Then, the crystals were taken out, washed 3 times with MilliQ water and dried with lens cleaning tissue. Next, the activated diamond surfaces were brought in contact with 200 μL Alexa 488 Cadaverine dye (Product number A30676, Thermo Scientific, the Netherlands) solution (100 μg/mL) in the 96-well plate. Incubation was performed overnight at room temperature while protecting the samples from the light. Then the diamond surfaces were taken out of the dye solution and washed with MilliQ water to remove any unattached dye. Excess solvent was removed by blowing the samples dry with nitrogen. All the surfaces were imaged using a laser scanning confocal microscope (Zeiss LSM780, Germany). The same microscope settings (Gain 1000 and laser power 3.5) where used for all the plates in the same experiment. We note that for imaging the Alexa 488 Cadaverine dye attached to the diamond surface via non-covalent simple adsorption, a higher gain and laser power was used. The fluorescence intensity of the surface was subsequently quantified using Zeiss Blue software.

2.3. Interaction with cell culture medium

The freshly cleaned diamond surfaces were placed in three different wells of the 48-well plates. Then 100 μL foetal bovine serum (FBS) was added to the each well followed by 900 μL DMEM-HG medium. After incubation at the room temperature for 30 min, the surfaces were taken out of the well, the extra medium on the diamond surface was carefully removed using a soft tissue and the surface was blown dry with nitrogen. The thickness of salt-protein layer on the diamond surface was measured by ellipsometry (EL X−02C, DRE, Ratzeburg, Germany) [38] in three different positions per surface and three measurements per position. During ellipsometry measurements, an incidence angle of 50° and a 632 nm laser were used. A home-built Matlab script was employed to compute the film thickness from the amplitude ratio (Ψ) and the

relative phase shift data (Δ). This entire experiment was repeated three times independently. We note that the accuracy of ellipsometer was also validated using atomic force microscopy.

2.4. Interaction of diamond crystals with bacteria

Precultures of *Staphylococcus aureus (S. aureus)* ATCC 12600 were prepared by suspending a colony in 10 mL sterile Tryptone Soy Broth (TSB) (Sigma OXOID, the Netherlands) and incubating at 37 °C in a shaker incubator at 150 rpm for 24 h. Then, a main culture was prepared by adding the preculture to the sterile TSB medium in the ratio 1:20 by volume followed by 16 h of incubation. Next, the cultures were washed twice with 10 mL sterile PBS alternated with centrifugation at 10 °C and 6500 rpm (Beckman Coulter JLA 16.250). After washing, the cultures were resuspended in the PBS, sonicated and number of bacteria in the suspension was quantified with a Bürker-Türk counting chamber. Cultures of *Escherichia coli (E. coli)* ATCC 8739 were prepared following an analogous protocol using Luria Bertani (LB) (Sigma OXOID, the Netherlands) medium and incubating the main culture for 20 h [39]. To assess the attachment of bacteria on the <100>, <110>, <111> diamond surfaces, the crystals were placed in a 48-well plate to which a *S. aureus* or *E. coli* suspension (3×10^4 CFU/mL) was added. After 5 h of incubation, the surfaces were removed from the bacteria suspension and washed by sterile PBS three times to remove non-adhered bacteria, before live-dead staining. Samples were stained in the wells with 200 μL BacLight Live/Dead viability stain containing a SYTO 9 dye (yielding green fluorescence in live organisms) and propidium iodide (yielding red fluorescence in cell membrane-damaged, dead organisms) (5 μM) (Invitrogen, Thermo Fisher Scientific, the Netherlands), followed by 15 min incubation in the dark. The images were recorded using a fluorescence microscope (Leica DM4000B, Germany) and the image analyzed using FIJI to quantify the number of the adhered bacteria per unit area of the surface. Three images were recorded at three different locations for every surface in each experiment. This experiment was repeated two times.

Furthermore, the effect of diamond surface chemistry on the bacterial adhesion was assessed by evaluating the attachment of *S. aureus* ATCC 12600 on reduced and pristine surfaces. Except for the surface treatment (which was achieved using the process described in section 2.1), the experimental protocol was exactly the same as mentioned above. In another experiment, to study the long-term stability of the diamond crystals towards bacterial repellency/adhesion, the oxidized diamond surfaces were incubated with an *S. aureus* ATCC 12600 suspension at 37 °C for 24 h. Post incubation, the surfaces were processed in the same fashion as described above.

2.5. Interaction of diamond crystals with HeLa cells

HeLa cells were cultured in DMEM-HG (Dulbecco's Modified Eagle Medium with 4500 mg/L glucose), supplied with 10% FBS , 1% Penicillin/streptomycin and 1% Glutamax at 37 °C and 5% CO_2. All the culture medium components were purchased from Gibco, Life Technologies, the Netherlands. To investigate the HeLa cell attachment on different diamond surfaces, 1 mL of a HeLa cell suspension (3×10^4 cells/mL) were added to the 48-well plate containing the diamond crystals. After 5 h (or 2 days) of incubation, the diamond crystals were washed 3 times with PBS to remove the unattached cells. Next, the adhered cells were fixed by incubating the diamond crystal in 4% paraformaldehyde solution for 15 min, followed by staining the cytoskeleton and nuclei using phalloidin-TRITC (2 μg/mL) and DAPI (4 μg/mL) (Invitrogen, Thermo Fisher Scientific, the Netherlands), respectively for 40 min. The surfaces were then imaged using a confocal microscope (Zeiss LSM780 NLO, Germany) followed by image analysis using FIJI to determine the number of cells attached per unit area of the surface. For experiments where cells were cultured on the crystals for 2 days, cells were only imaged using optical microscope for qualitative assessment (Leica DM IL LED, Germany) without any immunostaining and quantification.

2.6. Interaction of diamond crystals with primary cortical neurons

Primary cortical neurons were obtained from embryonic brains at embryonic day 14 of C57BL/6J pregnant mice. The cortices were dissected, the meninges removed and neurons were obtained from the cortices by mechanical dissociation. In order to prepare a single cell suspension, neurons were filtered through a 42 μm pore size filter. Neurons were plated on diamond crystals placed in the 96-well plates (without pre-coating) at a density of 0.3×10^6 cells/ml. As a standard control, cells were also plated on 96-well plates coated with polyethylenimine (PEI). In particular, a 96-well plate was incubated with 70 μL PEI/well overnight, followed by rinsing with MilliQ water. As culture medium for the neurons, neurobasal medium supplemented with 2% (v/v) B27, 0.25% (v/v) glutamine and 0.2% (v/v) penicillin/streptomycin was used. After 24 h, the neurons were treated with 10 μM cytosine arabinoside for 24 h more in order to prevent the growth of non-neuronal cells and assure a neuronal culture with 95% purity. Neurons were allowed to grow and develop in the neurobasal medium until day 7. Animal experimental procedures were approved according to the Dutch law by the local ethics committee (DEC 16630).

2.7. X-ray photoelectron spectroscopy

In order to understand the differences in interaction between biomolecules and the diamonds with different crystal orientations, we investigated the surface chemistry of all the crystals. Chemical composition of all the surfaces was characterized by X-ray photoelectron spectroscopy (XPS). We used two different XPS setups for the analysis. Initial XPS experiments to determine the amount of oxygen for different diamond crystals were performed using the following protocol. After acid cleaning and washing the plates with ultrapure water following the procedure explained in section 2.1, the diamond crystals were transferred to the XPS immediately (<5 min). XPS was conducted using an SSI S-Probe (Surface Science instrument, Mountain View, CA, USA) with a monochromatic Al Kα X-ray source (1486.8 eV). The pass energy is set at 150 eV for the survey spectra (survey spectra, C1*s*, O1*s*, C KLL) and to 50 eV for the detailed spectra of the C 1*s* and O1*s* core level regions. The spectra have been processed using the Hawk Data Analysis 7 software [40,41]. In a single experiment, atomic compositions of all the surfaces were quantified sequentially, where each surface was scanned three independent times and the results of the three scans were averaged. The same experiment was repeated two independent times.

XPS analysis to investigate the effect of different reactions on the surface termination of diamond crystals was performed using a Surface Science SSX-100 ESCA instrument with a monochromatic Al Kα X-ray source ($h\nu = 1486.6$ eV). This ultrahigh vacuum setup also has a preparation chamber with a sputter gun, where the pristine diamond surfaces were prepared *in situ* by bombarding the surface with 5 keV Ar ions for 10 min. The pressure in the measurement chamber was maintained below 1×10^{-9} mbar where the electron take-off angle with respect to the surface normal was maintained at 37°. The XPS data were acquired by using a spot size of 1000 μm diameter and the energy resolution was set to 1.3 eV for both the survey spectra and the detailed spectra of the C1*s*, N1*s*,

O1*s*, and Na1*s* core level regions. Furthermore, a gold mesh placed 1 mm above the sample was used during the XPS measurements in order to prevent the charging effect in addition to using an electron flood gun. Binding energies are reported ±0.1 eV and referenced to the C1*s* photoemission peak centered at a binding energy of 284.8 eV [42]. All XPS spectra were analyzed using the least-squares curve-fitting program Winspec (developed in the LISE laboratory of the Facultes Universitaires Notre-Dame de la Paix, Namur, Belgium). Deconvolution of the spectra included a Shirley [44] baseline subtraction and fitting with a minimum number of peaks consistent with the chemical structure of the sample, taking into account the experimental resolution. The profile of the peaks was taken as a convolution of Gaussian and Lorentzian functions. The uncertainty in the peak intensity determination is 2% for all core levels reported.

2.8. Atomic force microscopy

AFM scans of the diamond crystal surfaces were recorded on a BioScope Catalyst (Bruker) in contact mode using DNP tip (Bruker) at three different locations per crystal. Surfaces were acid cleaned just prior to the AFM imaging. The images were processed and analyzed using the Nanoscope Analysis 1.8 software; 1st order flattening was performed followed by the root mean squared surface roughness (Rq) quantification. We note that, exactly the same process was conducted on all the three surfaces.

3. Results and discussion

3.1. Surface structure and characterization

Fig. 1a depicts a schematic of the atomic arrangement of the <100>, <110> and <111> crystal surfaces, where red and white circles represent the carbon atoms in the top surface and in the crystal plane below, respectively. Bonds formed by the carbon atoms in the top plane and in the plane below are indicated by the green and yellow color respectively. It can be clearly seen that the number of carbon atoms in the unit lattice in the top surface and their bonding configuration vary depending on the crystal orientation. As mentioned earlier high pressure high temperature (HPHT) diamond crystals having <100>, <110> and <111> orientation at the exterior surfaces (Almax EasyLabs) were used in this work. First, three surfaces were cleaned in the boiling mixture of sulphuric and nitric acid followed by rinsing them with the MilliQ water [32,34]. Then, surface roughness was characterized using atomic force microscopy as shown in Fig. 1b. It was found that all the surfaces had similar surface roughness (<5 nm). Therefore, any differences observed in the interaction between the biological matter and the single crystal diamond can be attributed to the variations in the surface chemistry caused by the changes in surface orientations alone. Next, we investigated the influence of diamond's crystal orientation on the biological applications.

3.2. Biomolecule conjugation

Drug loading [22] or attaching an antibody of interest [45] on the diamond surface is routinely carried out in biological experiments. These molecules are typically attached using EDC-NHS coupling [46]. Hence, to explore the impact of the surface orientation on such biomolecule conjugation processes, we used the EDC-NHS reaction to attach a fluorescent molecule on the diamond surface. We used Alexa 488 cadaverine fluorescent molecule because its fluorescence allows a quantitative assessment of the attachment process. To perform the attachment, the carboxylic acid groups on the surface were converted into the succinimidyl ester complexes through EDC-NHS treatment, which then instantly reacted with Alexa 488 cadaverine molecules as shown in Fig. 2a. After the chemical reaction, surfaces were washed with ultrapure water to remove any unattached molecules. Then, surfaces were imaged using laser scanning confocal microscopy to image the surface fluorescence as shown in Fig. 2b along with the quantification of the fluorescence intensity determined using the ZEN-Blue

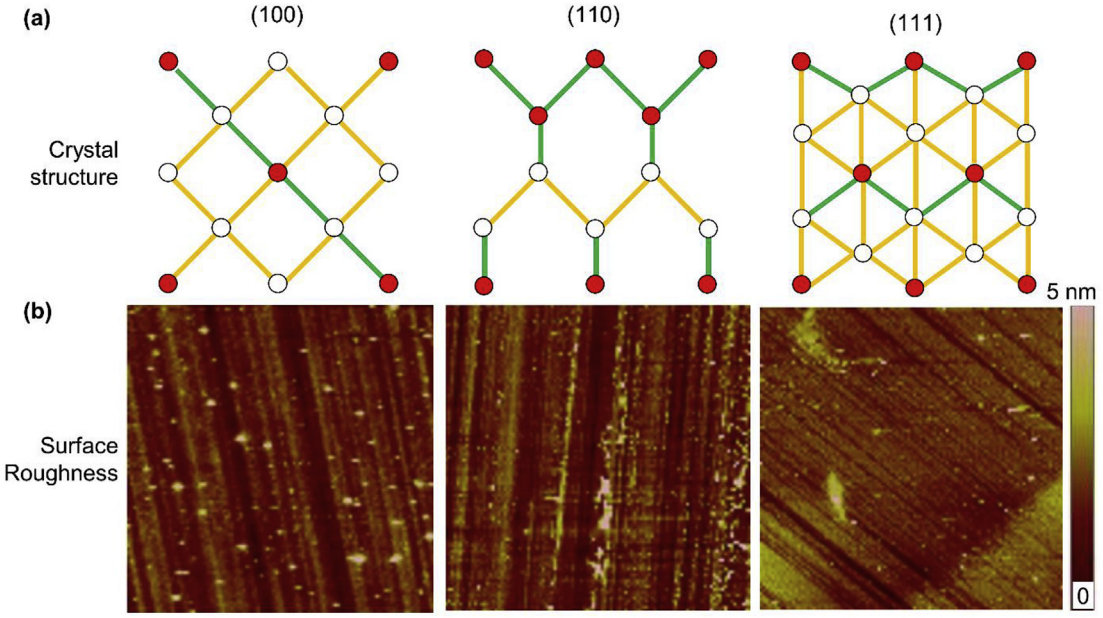

Fig. 1. (a) Schematic of the atomic arrangement and bonding of the top surface for different the lattice orientations of single crystal diamond as viewed from the top. The red circles indicate carbon atoms in the top surface. White circles represent the carbon atoms in the crystal plane below. Bonds formed by the carbon atom in the top plane and in the bulk crystal are indicated by the green and yellow color, respectively. (b) Topographic images collected by AFM illustrating the surface roughness of the three low index diamond surfaces. All the panels show AFM scans of 10 μm × 10 μm of the crystal surface. (A colour version of this figure can be viewed online.)

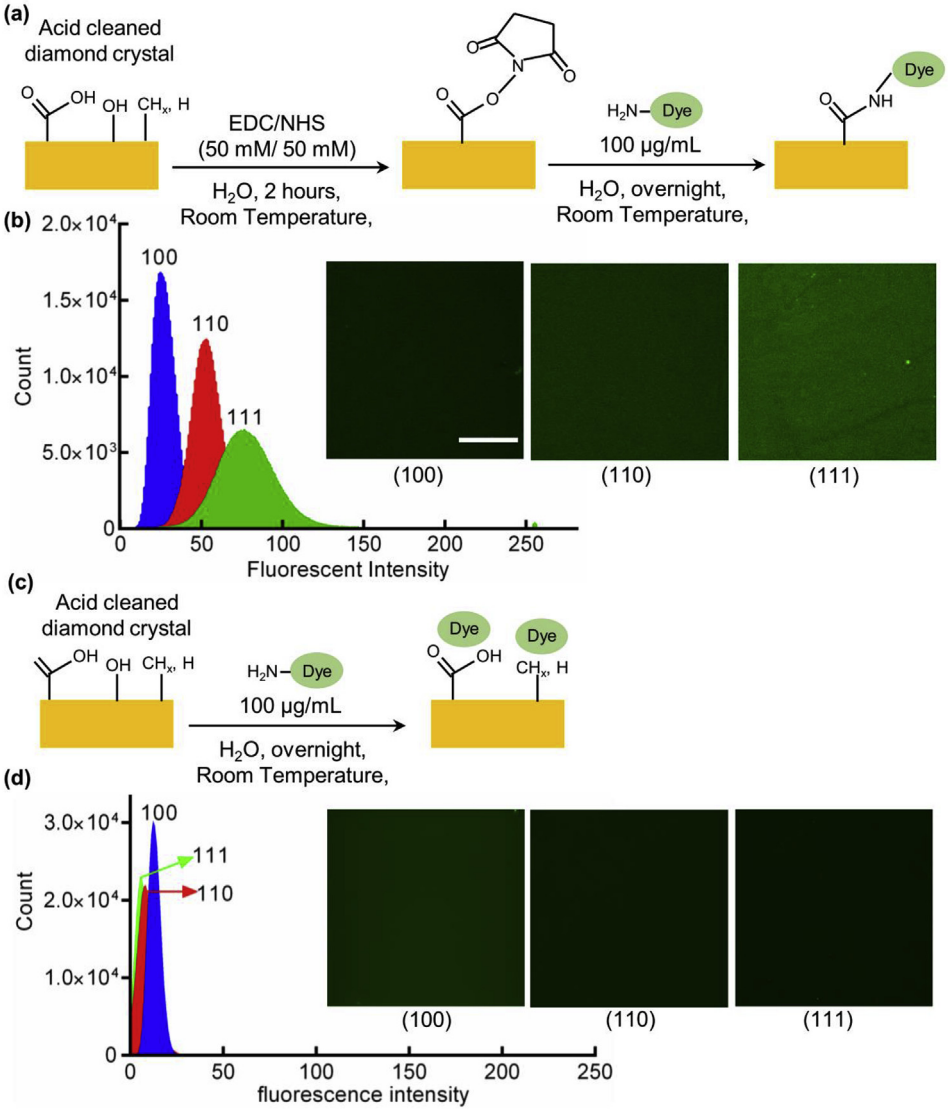

Fig. 2. Effect of different surface orientations on the covalent and non-covalent attachment of biomolecules on the diamond. (a) Different steps involved in the covalent conjugation of biomolecules to the diamond surface using EDC-NHS reaction. (b) Quantification of fluorescence intensity of Alexa 488 cadaverine molecules attached to the diamond surfaces. Confocal microscopy images of crystal surfaces are also shown (scale bar: 20 µm). Non-covalent adsorption of dye molecules on the diamond surfaces (c) gives rise to weak fluorescence(d). (A colour version of this figure can be viewed online.)

Edition image processing software (Zeiss). From these results, it is evident that the fluorescence, and hence the carboxylic acid groups on the surface, are most concentrated on the <111> surface, followed by the <110> and <100> surfaces. This result demonstrates the differences in the surface functionalization for the different surfaces post acid cleaning. These differences on the molecular level were found to alter the biomolecule conjugation reaction.

Oxidized diamond generated by the acid cleaning is known to have affinity towards biomolecules through hydrogen bonding, electrostatic or other polar interactions [46]. Therefore, we explored if there are any differences in non-covalent adsorption of the highly polar Alexa 488 cadaverine molecule for the plates with different surface orientations. In particular, we simply incubated the acid cleaned plates with the dye overnight (Fig. 2c) followed by washing the plates with MilliQ water and imaging. Results of this experiment are given in Fig. 2d. The trends in the fluorescence intensity were opposite compared to those observed in the experiments described above. However, it should be noted that the overall fluorescence intensity was significantly lower as compared to the covalent attachment. In fact, to make the fluorescence visible, higher laser power and gain settings (Image settings for dye adsorption without EDC/NHS: laser powder: 8.5 mW gain: 930 Image settings for Dye conjugation with EDC/NHS:laser powder: 3.5 mW gain: 1000) were used compared to the experiment described above. Therefore, non-covalent adsorption of the molecule on the diamond surfaces with different orientations was determined to be negligible.

3.3. Interaction with cell culture medium

As single crystal diamonds are used for cell culturing and nanodiamonds are investigated as intracellular sensors, more insights into the interaction between the cell culture medium and the bulk- or nano-diamond surfaces is necessary. Hemelaar et al. recently showed that salts and proteins from cell culture medium form a corona on nanodiamonds [47], which has a flake-like shape. The preferred crystallographic orientation of the main facet is in the (110) direction [48]. In fact, this corona leads to the aggregation of

nanodiamonds, which can hinder their cellular uptake. Therefore, we explored whether different diamond facets interact differently with the cell culture medium via investigating the thickness of the dry protein-salt film on the diamond surface. In particular, post acid boiling diamond crystals were first immersed in the 0.1 mL fetal bovine serum (FBS) and then 0.9 mL Dulbecco's Modified Eagle Medium-high glucose (DMEM-HG) complete medium was added on the crystals. This protocol is similar to the one used for transporting nanodiamonds inside mammalian cells [47]. After 30 min of incubation, excess medium on the diamond plates was carefully removed using a soft tissue paper touching only the edges of the plates. The diamond crystals were blown dry with nitrogen for ~15 s and the protein film thickness was measured non-invasively using ellipsometry. The ellipsometry results shown in Fig. 3 indicate that the thickness of the dried protein-salt film on the <100> surface was ~76 nm, i.e. significantly higher than on the <110> (~58 nm) and the <111> surface (~46 nm). This suggests that the <111> diamond surface inherently reduces corona formation as compared to the <100> and <110> planes.

3.4. Bacterial attachment

Diamond coatings or diamond crystals with a specific dopant such as boron have been investigated for their anti-biofouling property [13,14]. Hence, we also investigated if any particular diamond surface inherently repels bacteria. Here, we incubated the diamond plates with a bacterial suspension of *Staphylococcus aureus* (*S. aureus*, ATCC 12600) or *Escherichia coli* (*E. coli*, ATCC 8739) bacteria (chosen as representatives of Gram-positive and Gram-negative bacteria, respectively). After 5 h of incubation, the diamond crystals were washed to remove any non-adhered bacteria, and live-dead staining was performed. The diamond surfaces were then imaged with a fluorescence microscope to determine the average density of adhered live and dead bacteria (indicated by green and red fluorescence, respectively), as shown in Fig. 4. We note that almost no dead bacteria could be observed on any of the surfaces. We found that both bacterial strains adhered densely on

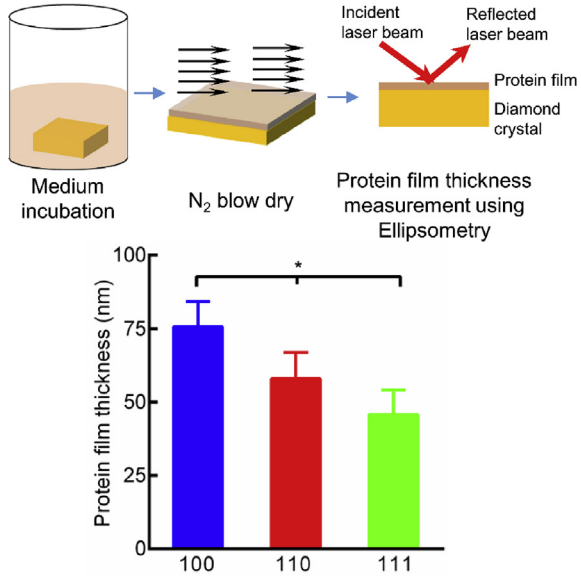

Fig. 3. Thickness of dry proteins-salts corona on <100>, <110> and <111> diamond surfaces as measured by ellipsometry. * denotes the statistical significance as determined by the one-way Anova test calculated from 9 different measurements recorded during 3 experiments. The error bar shows the standard deviation. (A colour version of this figure can be viewed online.)

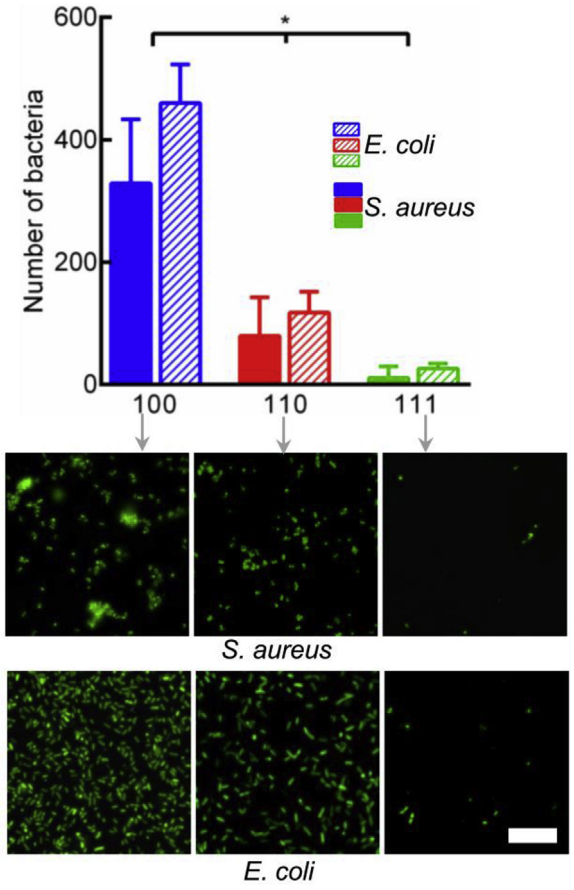

Fig. 4. Attachment of *S. aureus* and *E. coli* bacteria on diamond crystals with different surface orientations. The scale bar indicates 15 μm * indicates statistical significance as determined by the one-way Anova test (~15–20 different measurements). The error bar shows the standard deviation. (A colour version of this figure can be viewed online.)

the <100> surface, whereas the <111> surface showed nearly no bacterial coverage. However, although this trend was similar for both bacterial strains, the absolute number of bacteria attached to the surface was different. Specifically, *S. aureus* showed lower surface coverage than *E. coli*. It is known that both bacteria have negative surface charge, with *E. coli* being less negative compared to *S. aureus* [49]. Since surface roughness, wettability and other mechanical properties were similar for all three surfaces, differences in bacterial adhesion point to a possible role of the net surface charge of the crystal surface in mediating interaction with bacteria. Furthermore, differences in the functional groups on the three surfaces, as revealed by the biomolecule conjugation experiments, may also be the underlying cause of the differences in bacterial adhesion.

3.5. Effect of surface termination and incubation time on bacterial adhesion

In the bacterial adhesion experiments described above, the diamond plates had oxygen terminated surfaces resulting from the acid cleaning. We also investigated if the bacterial attachment depends on the surface chemistry of the diamond plates and if the preferential bacterial adhesion on <100> plane is dependent on the chemical groups grafted to the surface. To do this, we modified the surface chemistry of all the diamond plates by subjecting them to either to a BH_3-THF reduction reaction to obtain the reduced

surface chemistry or to argon ion sputtering to produce a pristine surface. These diamond plates were incubated with a *S. aureus* bacterial suspension for 5 h. Post-incubation the plates were washed to remove any non-adhered bacteria, live-dead stained and imaged as explained section 3.4. Results of this experiment are shown in Fig. 5a. We observed that bacterial adhesion was strongest for oxygen-terminated (acid cleaned) diamond, followed by hydrogen-terminated (reduced) and weakest on the nearly pristine surface. Furthermore, the <100> diamond surface was found to be the most sensitive to surface chemistry as far as *S. aureus* bacterial attachment is concerned, whereas the <111> surface was the least sensitive. In fact, the <111> surface showed nearly no bacterial attachment for all three surface treatments.

Next, we studied the "bacterial repellency" of the three diamond surfaces as a function of time since functional stability over a long duration is of key importance in the case of antimicrobial surfaces. We incubated the oxidized diamond crystals with a *S. aureus* bacterial suspension for a day instead of for only 5 h and studied the surfaces using the same protocol as explained earlier. The results of this experiment are shown in Fig. 5b and clearly highlight that the <111> surface of diamond remains more bacteria repellent after 24 h than the <100> and <110> surfaces. The absolute amount of bacterial adhesion compared to 5 h of bacterial incubation was higher for all the three surfaces as expected. These results demonstrate both short and long term surface orientation dependent preferential bacterial adhesion/repellency.

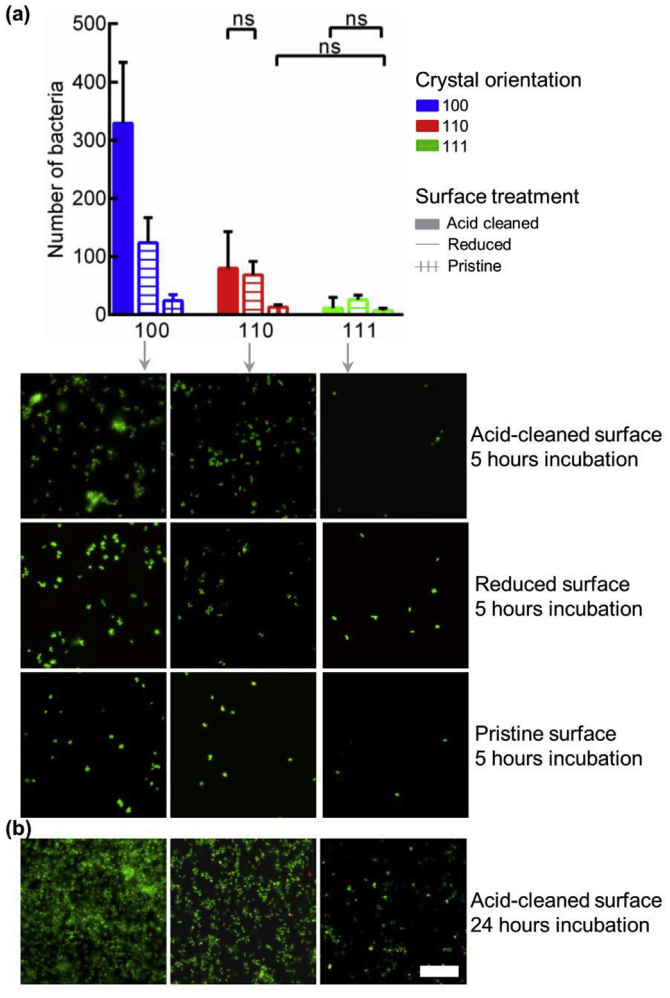

Fig. 5. (a) Attachment of *S. aureus* bacteria on the <100>, <110> and <111> surfaces of diamond. The scale bar indicates 15 μm. All the groups in the figure have statistically significant difference except the three groups marked in the figure as determined by the one-way Anova test conducted on ~15–20 different measurements. The error bars show the standard deviation. (b) Acid cleaned oxidized diamond crystals after incubation in a *S. aureus* bacteria suspension for 24 h. (A colour version of this figure can be viewed online.)

3.6. Mammalian cell attachment

To investigate if the diamond surface orientation influences the interaction with mammalian cells, we determined the adhesion and proliferation of HeLa cells on them. HeLa is the most widely used cell line to investigate human cell and molecular biology [47,50]. Here, we seeded 30,000 HeLa cells on the diamond surfaces placed in 48 well plates. After 5 h during which the cells could attach to the diamonds, the surfaces were washed with PBS, followed by fixing, staining and imaging using the protocols described in the literature [47]. From the images, we quantified the density of cells attached to the surface. As shown in Fig. 6a, we observed that fewer cells adhered to the <100> surface than to the <110> surface, which in turn showed a lower cell density than the <111> surface. Interestingly, this trend is opposite to that for bacterial adhesion. However, the difference in the average number of cells on the three surfaces was not statistically significant when tested with a one-way Anova test.

We also investigated if HeLa cell adhesion varies for longer culture times and for this, we cultured HeLa cells on the diamond surfaces for two days using the same protocol detailed above. The results of the experiment are reported in the SI: a confluent cell layer was detected on all the three surfaces. Therefore we can conclude that the differences in density of grafted HeLa cells on the three diamond surface orientations observed for short culturing times do not influence the cell coverage after long culture times, and this coverage is the same for the three low index surfaces.

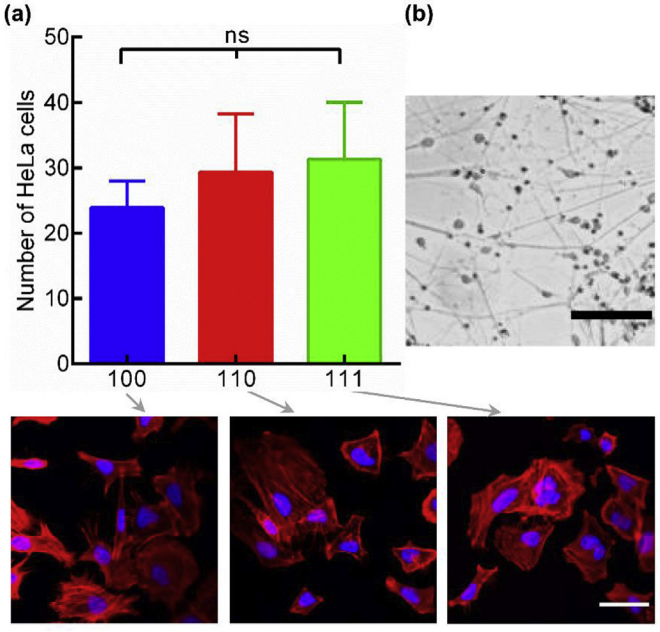

Fig. 6. (a) Adhesion of HeLa cells on <100>, <110> and <111> diamond surfaces. The confocal images in the bottom row are representative for the respective plates (scale bar: 50 μm) where cytoskeleton and nuclei were stained using phalloidin-TRITC and DAPI, respectively. (b) Neurons attached on the unmodified, acid cleaned and sterilized <110> diamond surface; the image was recorded by a wide field optical microscope (scale bar: 100 μm). (A colour version of this figure can be viewed online.)

Our last adhesion experiment concerned primary cortical neurons harvested from embryonic brains at embryonic day 14 of C57BL/6J pregnant mice [51]. This study was triggered by the fact that the superior biocompatibility, electric properties and quantum coupled optomagnetic properties of the nitrogen-vacancy (NV) defect sites of diamond make it an attractive material for neuronal research. For instance, detecting the neuronal action potential using the quantum sensing ability of NV defect centers in diamond has been proposed [52]. On the other hand, Hall and co-workers exploited NV centers to image neuronal activity with high spatio-temporal resolution [53]. Surfaces coated with nanodiamonds [3], nanocrystalline diamond films [4] and chemically patterned single crystal diamond [5] have also been used to culture neurons. Here, we investigated if neurons can attach and grow on the diamond surface and if they have any preferential affinity towards a particular low index surface by seeding ~60,000 cells on the diamond surfaces. 24 h postseeding, the neurons were treated with 10 μM cytosine arabinoside for 24 h in order to prevent the growth of non-neuronal cells. Then neurons were further allowed to grow and develop in the neurobasal medium until day 7 when cells were imaged with the light microscope as shown in Fig. 6b. We observed that neurons showed identical affinity towards the different low index diamond surfaces. Observing the morphology with microscopy leads to the conclusion that neurons grow and develop on diamond surfaces in a comparable fashion to the standard culture on cell culture plates coated with polyethylenimine. However, in a few places on all crystals, neurons were found to form aggregates similar to those observed by Babchenko et al. [7] even if in our case the diamond plates were not coated.

3.7. Theoretical calculations

To better understand the experimentally observed behavior, we performed first principle calculations for the <100>, <110>, and <111> surfaces of diamond with various surface terminations (clean, −H, −F, −O, and −OH). Here, “clean” indicates the hypothetical case where no functional groups are present on the diamond surface. Results of these calculations (as presented in the SI) clearly indicate that all the functional groups stabilize the surface compared to the “clean” surface. Next, we calculated the charge distribution at these surfaces using the Hirshfeld-I partitioning scheme [54,55]. As shown in Fig. 7, a strong dipole is found to form between the diamond surface and the surface terminating groups, similar to that seen in defects in diamond [56]. Moreover, a dipole is also formed within the top layers of the system. However, the charges for the layers below the 4th C layer show bulk behavior (*i.e.*, nearly zero charge).

Furthermore, in the case of oxygenated diamond, the charge on the oxygen atom is heavily dependent on the surface orientation as shown in Table 1. In particular, the charge on the oxygen atom on the <100> surface is 2−4 times that on the <110> and <111> surfaces. This difference probably originates from the formation of a double bond on the <100> surface, in contrast to the single bond for the <110> and <111> surfaces. As the diamond crystals used in this work were acid-cleaned, the top surface is expected to be oxygen-terminated [57]. Therefore based on these calculations, the different low index surfaces of diamond are expected to show a different reactivity due the variation in the charge on the oxygen atom.

3.8. X-ray photoelectron spectroscopy

We experimentally characterized the atomic composition of all the low index diamond surfaces with different surface terminations using XPS. In the SI, Fig. S3 shows the XPS spectra of the C1*s* core level region of the three acid-treated low index diamond surfaces.

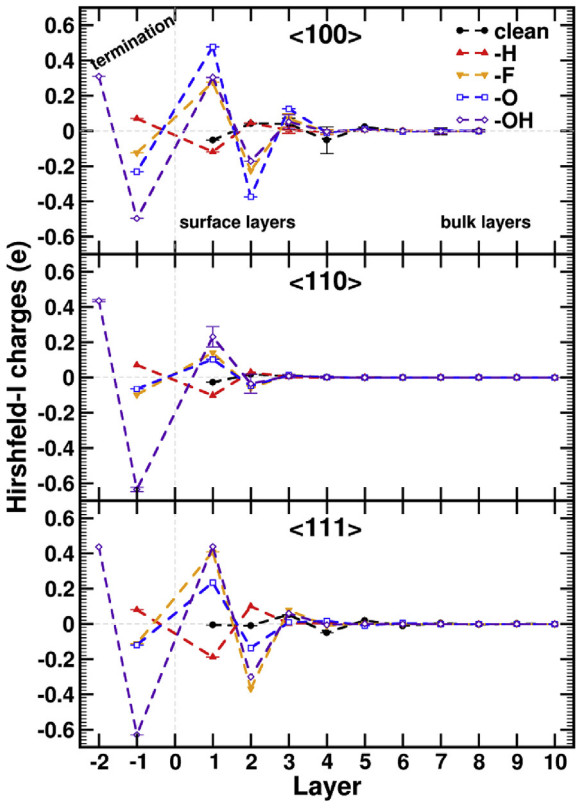

Fig. 7. Averaged atomic Hirshfeld-I charges as function of layer depth for the different (terminated) surfaces. The standard deviation is shown as error bars. The surface termination atoms (H, F, and O) are indicated as layer −1. For the hydroxyl termination, the H is indicated as layer −2, while the O is indicated as layer −1. The bulk layers are the layers at the center of the symmetric slab models. (A colour version of this figure can be viewed online.)

From these data and from the spectral intensities of the O1*s* and Na1*s* lines we deduced the elemental composition of the surfaces before and after BH_3-THF reduction. The fit of the C1*s* spectra allowed us to determine the various surface functional groups and determine their relative abundance on the surfaces before and after BH_3-THF reduction, as detailed in the SI for the case of the <100> surface. In the SI we report the XPS survey spectra for the three low index diamond surfaces (Fig. S4) after the various surface treatments, as well as the detailed spectra of the C1*s*, N1*s*, O1*s* and Na1*s* core level regions obtained for the same surfaces (Fig. S5).

Here we present the results of the analysis of these spectra. The relative oxygen concentrations as deduced from the detailed core level spectra collected from the three low index surfaces after acid cleaning is reported in Fig. 8a. Fig. 8b lists the different functional groups present on the three diamond surfaces as identified from the detailed C1*s*, N1*s* and O1*s* spectra. Results of the XPS analysis revealed that >95% of the surface analyzed was made up of carbon and oxygen, which is expected for a diamond crystal. However, small amounts of sodium (<3%) were also found on the diamond surface. Despite the fact that the samples where all acid-cleaned before analysis, these traces might come from residues that we could not remove during the cleaning or that were present in the cleaning solutions themselves. XPS measurements were repeated three independent times. In one of the measurements, traces of silicon (<1%) were also found. Silicon could have appeared from the cleaning process or from the impurities trapped in the bulk diamond. However, the latter possibility is far more likely than the prior because silicon is known to be one of the most prominent

Table 1
Hirshfeld-I charges [e] of the surface layers of oxygen terminated diamond. Charges are per atom.

Surface orientation	Oxygen terminated surface	Carbon atom layer 1	Carbon atom layer 2
<100>	−0.232	0.477	−0.375
<110>	−0.059	0.090	−0.040
<111> (1x1)	−0.090	0.223	−0.163

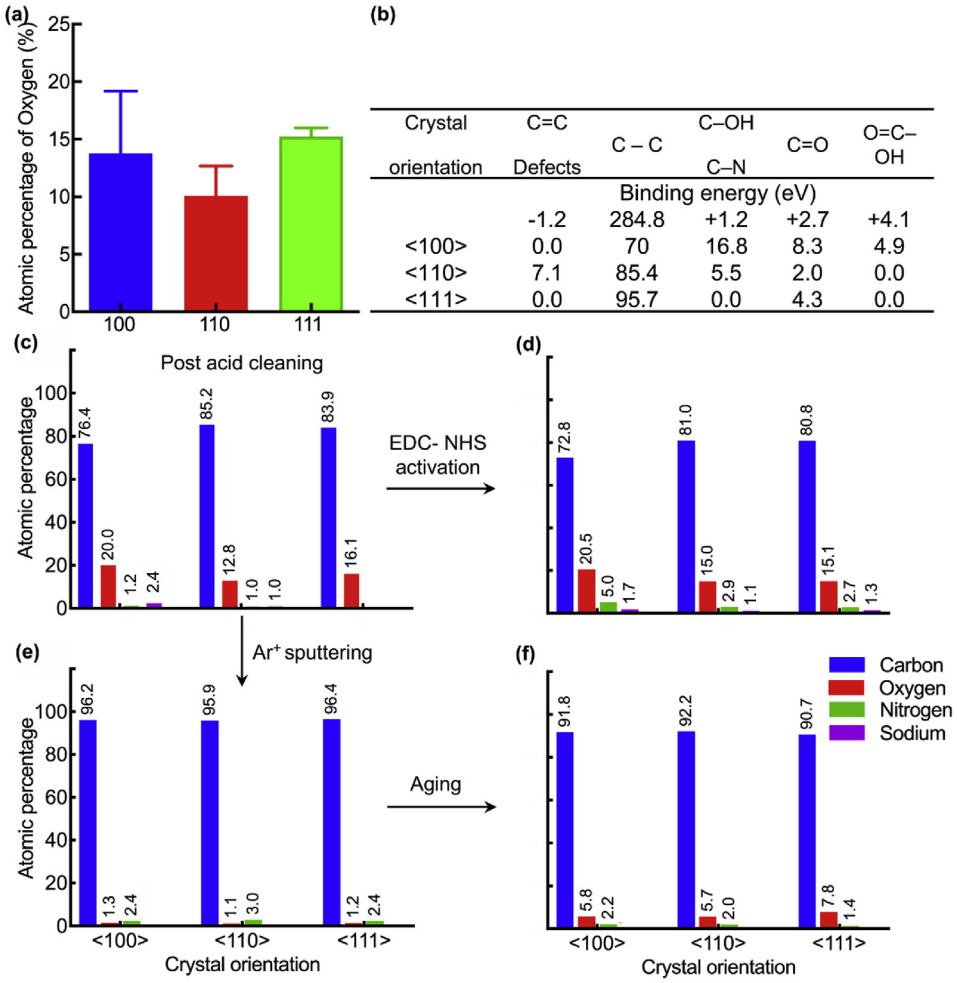

Fig. 8. (a) Amount of oxygen on the <100>, <110> and <111> surfaces of diamond after acid treatment; (b) different surface functional groups and (c–f) difference in atomic composition post surface treatments for the three low index diamond surfaces. (A colour version of this figure can be viewed online.)

impurities in the diamond crystal. We note that, elements present in atomic percentages of less than 0.2 were disregarded.

As shown in Fig. 8a, after acid treatment the oxygen content was highest on the <111> surfaces whereas it was lowest for <110> surfaces. This result highlights how the degree of surface oxygenation can vary due to the differences in crystal orientation alone although all the crystals underwent exactly the same acid treatment. Furthermore, we probed the differences in the functional groups generated on the different diamond surfaces as a result of acid oxidation using XPS, which are presented in Fig. 8b. Peak fitting carried out for functional group identification is presented in Fig. S3 of the SI. Here, we assigned the 284.8 eV binding energy component to C–C throughout our analysis and components at a shifted binding energy (BE) were attributed to the presence of functional groups. Specifically, shifted by -1.2 eV we find the component assigned to C=C/defects [32,40,58]; shifted by +1.2 eV the spectral signature of C–OH/C–N [59,60]; at +2.7 eV higher BE the contribution of C=O [32] moieties, and at +4.1 eV higher BE that of O=C–OH [58,59]groups. We would like to point out that the energy shift of +4.1 eV, which we assigned to carboxylic acid groups is lower than the typical values of +4.5 - +4.8 eV reported in the literature. This result clearly demonstrates the qualitative variation in the abundance of functional groups on the different low index diamond surfaces after acid oxidation. Here, the XPS results showed the highest amount of carboxylic groups on <100> surface. On the other hand, the same surface showed the least fluorescence in biomolecule conjugation experiments.

Next, we analyzed the XPS results of the reduced, EDC-NHS activated or pristine diamond surfaces (Fig. S5) in order to determine the relative abundance of functional groups in each case. As detailed above in the experimental section, reduced and EDC-NHS treated surfaces were obtained after treating the surfaces with BH_3-THF solution, followed by hydrolysis with hydrochloric acid or EDC–NHS reaction respectively. To obtain the “pristine” diamond

surface, the crystal surface was bombarded with argon ions *in situ*. The "aged" surfaces were realized by taking the pristine diamond surfaces out of the XPS equipment and allowing them to "age" in a plastic tube under ambient conditions. Here, our goal was to evaluate through the XPS analysis if different surface orientations of the diamond crystal have different affinity for oxygen and nitrogen from the environment. The atomic composition of the reduced, EDC-NHS activated, pristine and aged diamond surfaces as obtained from the XPS core level intensities is given in Fig. 8c–f. As expected, we can clearly see the increase in nitrogen concentration for diamond surfaces after undergoing EDC–NHS treatment. For the pristine surface, small amounts of nitrogen and oxygen could be detected in addition to a large portion of carbon. Post aging, the atomic composition of the surfaces was found to vary compared to the pristine surfaces. Specifically, the increase in atomic percentage of oxygen was maximum for the <111> surface whereas very similar values were found for the <110> and <100> surfaces. This result corroborates the trend of oxygen amount found on the acid cleaned surface. Hence it can be concluded that the <111> surface shows a higher overall affinity for oxygen.

4. Conclusions

Here the effect of the crystal orientation of specific diamond low index planes on their interaction with biological matter was investigated. Moreover, this is the first report, which systematically investigates a broad spectrum of biological mater interacting with any crystalline material. In all previous studies, the interaction between either proteins or cells or bacteria or their combinations with various crystal planes of the specific material other than diamond was studied. The <100>, <110> and <111> diamond surfaces underwent the same oxidation treatment and showed comparable roughness under AFM. However, XPS showed that the degree of oxygenation of those surfaces and the resulting surface functional groups were different. Based on the Hirshfeld-I charge calculations, we theoretically determined that the amount of the surface charge and found that it is expected to vary depending on the surface orientation. Ultimately, these surface charges, oxygenation and the functional groups lead to the alteration in the interaction of biological matter with these surfaces. Specifically, <111> surface showed more efficient EDC-NHS conjugation than the other surfaces. This same surface orientation exhibited the highest inherent ability to repel *S. aureus* and *E. coli* bacteria. Furthermore, when investigating the interaction between different surfaces and cell culture medium, <111> surfaces showed the least dry protein-salt corona thickness. On the other hand, the average number of HeLa cells attached to the <100> surface was least among the three, although not statistically significant. In addition, from the neuronal cultures on the acid cleaned and sterilized single crystal , we showed that neurons were able to attach and proliferate equally on all the three low index surfaces. It is known that the culture of primary neuronal cells is challenging and neuronal culture surfaces need to be carefully engineered. For example, neuronal cells require primary amine groups on the culture surface [61]. The ease of culturing primary neurons, i.e., electrically excitable cells, on unmodified diamond surfaces is of significant importance to the neuroscience community. Furthermore, this work also opens up new avenues for the biological applications of nanodiamonds. In particular, if biomolecules show a preferential adsorption on a specific crystal surface, this could be useful when working with nanodiamonds. When using NV centers for sensing, one could attach drugs or antibodies either on the surface where the NV center is most sensitive or away from it.

Funding sources

This work is financially supported by Romana Schirhagl's European Research Council grant (ERC STG - 714289) and a FOM projectruimte (G-36). Additionally, Viraj Damle was supported by a Marie Curie Individual Postdoctoral Fellowship (DLV-838494) Kaiqi Wu by a CSC scholarship, and Aryan Morita by an LPDP grant. The computational resources and services used in this work were provided by the VSC (Flemish Supercomputer Center), funded by the Research Foundation-Flanders (FWO) and the Flemish Government - department EWI.

All of the imaging from this work was performed at the UMCG Imaging and Microscopy Center (UMIC).

Declaration of competing interest

The authors declare that they have no known competing financial interests or personal relationships that could have appeared to influence the work reported in this paper.

CRediT authorship contribution statement

Viraj Damle: Writing - original draft. **Kaiqi Wu:** Formal analysis. **Oreste De Luca:** Formal analysis. **Natalia Ortí-Casañ:** Data curation. **Neda Norouzi:** Formal analysis, Data curation. **Aryan Morita:** Data curation. **Joop de Vries:** Formal analysis. **Hans Kaper:** Formal analysis. **Inge S. Zuhorn:** Conceptualization. **Ulrich Eisel:** Supervision. **Danny E.P. Vanpoucke:** Software. **Petra Rudolf:** Formal analysis. **Romana Schirhagl:** Writing - original draft.

Appendix A. Supplementary data

Supplementary data to this article can be found online at https://doi.org/10.1016/j.carbon.2020.01.115.

References

[1] R.J. Narayan, R.D. Boehm, A.V. Sumant, Medical applications of diamond particles & surfaces, Mater. Today 14 (2011) 154–163, https://doi.org/10.1016/S1369-7021(11)70087-6.
[2] C.C. Wachesk, C.A.F. Pires, B.C. Ramos, V.J. Trava-Airoldi, A.O. Lobo, C. Pacheco-Soares, F.R. Marciano, N.S. Da-Silva, Cell viability and adhesion on diamond-like carbon films containing titanium dioxide nanoparticles, Appl. Surf. Sci. 266 (2013) 176–181, https://doi.org/10.1016/j.apsusc.2012.11.124.
[3] A.C. Taylor, C.H. González, B.S. Miller, R.J. Edgington, P. Ferretti, R.B. Jackman, Surface functionalisation of nanodiamonds for human neural stem cell adhesion and proliferation, Sci. Rep. 7 (2017) 1–11, https://doi.org/10.1038/s41598-017-07361-y.
[4] S.M. Ojovan, M. McDonald, N. Rabieh, N. Shmuel, H. Erez, M. Nesladek, M.E. Spira, Nanocrystalline diamond surfaces for adhesion and growth of primary neurons, conflicting results and rational explanation, Front. Neuroeng. 7 (2014) 1–9, https://doi.org/10.3389/fneng.2014.00017.
[5] C.G. Specht, O.A. Williams, R.B. Jackman, R. Schoepfer, Ordered growth of neurons on diamond, Biomaterials 25 (2004) 4073–4078, https://doi.org/10.1016/j.biomaterials.2003.11.006.
[6] A. Voss, S.R. Stateva, J.P. Reithmaier, M.D. Apostolova, C. Popov, Patterning of the surface termination of ultrananocrystalline diamond films for guided cell attachment and growth, Surf. Coating. Technol. 321 (2017) 229–235, https://doi.org/10.1016/j.surfcoat.2017.04.066.
[7] O. Babchenko, N. Romanyuk, P. Jendelova, A. Kromka, Tailoring morphologies of diamond thin films for neural stem cells culturing, Phys. Status Solidi Basic Res. 250 (2013) 2717–2722, https://doi.org/10.1002/pssb.201300082.
[8] T.L. Lasseter, B.H. Clare, N.L. Abbott, R.J. Hamers, Covalently modified silicon and diamond surfaces: resistance to nonspecific protein adsorption and optimization for biosensing, J. Am. Chem. Soc. 126 (2004) 10220–10221, https://doi.org/10.1021/ja047642x.
[9] T.L. Clare, B.H. Clare, B.M. Nichols, N.L. Abbott, R.J. Hamers, Functional monolayers for improved resistance to protein adsorption: oligo(ethylene glycol)-modified silicon and diamond surfaces, Langmuir 21 (2005) 6344–6355, https://doi.org/10.1021/la050362q.
[10] R.J. Hamers, W. Yang, O. Auciello, J.E. Butler, DNA-modified NCD thin films as stable, biologically active substrates, Nat. Mater. 1 (2002) 253–258, https://doi.org/10.1038/nmat779.Diamond.

[11] M. Alcaide, S. Papaioannou, A. Taylor, L. Fekete, L. Gurevich, V. Zachar, C.P. Pennisi, Resistance to protein adsorption and adhesion of fibroblasts on nanocrystalline diamond films: the role of topography and boron doping, J. Mater. Sci. Mater. Med. 27 (2016), https://doi.org/10.1007/s10856-016-5696-3.

[12] J.M. Garguilo, B.A. Davis, M. Buddie, F.A.M. Köck, R.J. Nemanich, Fibrinogen adsorption onto microwave plasma chemical vapor deposited diamond films, Diam. Relat. Mater. 13 (2004) 595–599, https://doi.org/10.1016/j.diamond.2003.10.008.

[13] J. Budil, P. Matyska Lišková, A. Artemenko, E. Ukraintsev, I. Gordeev, J. Beranová, I. Konopásek, A. Kromka, Anti-adhesive properties of nanocrystalline diamond films against Escherichia coli bacterium: influence of surface termination and cultivation medium, Diam. Relat. Mater. 83 (2018) 87–93, https://doi.org/10.1016/j.diamond.2018.02.001.

[14] O. Dunseath, E.J.W. Smith, T. Al-Jeda, J.A. Smith, S. King, P.W. May, A.H. Nobbs, G. Hazell, C.C. Welch, B. Su, Studies of Black Diamond as an antibacterial surface for Gram Negative bacteria: the interplay between chemical and mechanical bactericidal activity, Sci. Rep. 9 (2019) 1–10, https://doi.org/10.1038/s41598-019-45280-2.

[15] R.E. Wilson, I. Stoianov, D. O'Hare, Biofouling and in situ electrochemical cleaning of a boron-doped diamond free chlorine sensor, Electrochem. Commun. 71 (2016) 79–83, https://doi.org/10.1016/j.elecom.2016.08.015.

[16] C.-C. Fu, H.-Y. Lee, K. Chen, T.-S. Lim, H.-Y. Wu, P.-K. Lin, P.-K. Wei, P.-H. Tsao, H.-C. Chang, W. Fann, Characterization and application of single fluorescent nanodiamonds as cellular biomarkers, Proc. Natl. Acad. Sci. Unit. States Am. 104 (2007) 727–732, https://doi.org/10.1073/pnas.0605409104.

[17] T. Sekiguchi, S. Sotoma, Y. Harada, Biophysics and Physicobiology inside a single cell, Biophys. Physicobiology. 15 (2018) 229–234, https://doi.org/10.2142/biophysico.15.0.

[18] T. Rendler, J. Neburkova, O. Zemek, J. Kotek, A. Zappe, Z. Chu, P. Cigler, J. Wrachtrup, Optical imaging of localized chemical events using programmable diamond quantum nanosensors, Nat. Commun. 8 (2017) 14701, https://doi.org/10.1038/ncomms14701.

[19] M. Fujiwara, R. Tsukahara, Y. Sera, H. Yukawa, Y. Baba, S. Shikata, H. Hashimoto, Monitoring spin coherence of single nitrogen-vacancy centers in nanodiamonds during pH changes in aqueous buffer solutions, RSC Adv. 9 (2019) 12606–12614, https://doi.org/10.1039/c9ra02282a.

[20] M. Chipaux, K.J. Van Der Laan, S.R. Hemelaar, M. Hasani, T. Zheng, R. Schirhagl, Nanodiamonds and their applications in cells, Small 14 (2018), 1704263, https://doi.org/10.1002/smll.201704263.

[21] K.J. van der Laan, J. Naulleau, V.G. Damle, A. Sigaeva, N. Jamot, F.P. Perona Martinez, M. Chipaux, R. Schirhagl, Towards using fluorescent nanodiamonds to study chronological ageing in Saccharomyces cerevisiae, Anal. Chem. 90 (2018) 13506–13513, https://doi.org/10.1021/acs.analchem.8b03431.

[22] X. Zhang, R. Lam, X. Xu, E.K. Chow, H. Kim, D. Ho, Multimodal nanodiamond drug delivery carriers for selective targeting , imaging , and enhanced chemotherapeutic efficacy, Adv. Mater. 23 (2011) 4770–4775, https://doi.org/10.1002/adma.201102263.

[23] D. Ho, C.K. Wang, E.K. Chow, Nanodiamonds : the intersection of nanotechnology , drug development , and personalized medicine, Sci. Adv. 1 (2015), e1500439.

[24] A. Krueger, D. Lang, Functionality is key: recent progress in the surface modification of nanodiamond, Adv. Funct. Mater. 22 (2012) 890–906, https://doi.org/10.1002/adfm.201102670.

[25] R. Schirhagl, K. Chang, M. Loretz, C.L. Degen, Nitrogen-vacancy centers in diamond: nanoscale sensors for physics and biology, Annu. Rev. Phys. Chem. 65 (2014) 83–105, https://doi.org/10.1146/annurev-physchem-040513-103659.

[26] Z. Zhuang, M. Aizawa, Protein adsorption on single-crystal hydroxyapatite particles with preferred orientation to a(b)- and c-axes, J. Mater. Sci. Mater. Med. 24 (2013) 1211–1216, https://doi.org/10.1007/s10856-013-4879-4.

[27] K. Wang, C. Zhou, Y. Hong, X. Zhang, A review of protein adsorption on bioceramics, Interface Focus 2 (2012) 259–277, https://doi.org/10.1098/rsfs.2012.0012.

[28] Z. Zhuang, T.J. Fujimi, M. Nakamura, T. Konishi, H. Yoshimura, M. Aizawa, Development of a,b-plane-oriented hydroxyapatite ceramics as models for living bones and their cell adhesion behavior, Acta Biomater. 9 (2013) 6732–6740, https://doi.org/10.1016/j.actbio.2013.02.001.

[29] S. Faghihi, F. Azari, J.A. Szpunar, H. Vali, M. Tabrizian, Titanium crystal orientation as a tool for the improved and regulated cell attachment, J. Biomed. Mater. Res. 91 (2009) 656–662, https://doi.org/10.1002/jbm.a.32275.

[30] D. Hanein, H. Sabanay, L. Addadi, B. Geiger, Selective interactions of cells with crystal surfaces Implications for the mechanism of cell adhesion, J. Cell Sci. 288 (1993) 275–288.

[31] S. Ndlovu, A.J. Monhemius, The influence of crystal orientation on the bacterial dissolution of pyrite, Hydrometallurgy 78 (2005) 187–197, https://doi.org/10.1016/j.hydromet.2005.03.004.

[32] X. Wang, A.R. Ruslinda, Y. Ishiyama, Y. Ishii, H. Kawarada, Higher coverage of carboxylic acid groups on oxidized single crystal diamond (001), Diam. Relat. Mater. 20 (2011) 1319–1324, https://doi.org/10.1016/j.diamond.2011.08.011.

[33] L. Xie, T.X. Zhou, R.J. Stöhr, A. Yacoby, Crystallographic orientation dependent reactive ion etching in single crystal diamond, Adv. Mater. 1705501 (2018), 1705501, https://doi.org/10.1002/adma.201705501.

[34] J. Kleinlein, T. Borzenko, F. Munzhuber, J. Brehm, T. Kiessling, L.W. Molenkamp, NV-center diamond cantilevers: extending the range of available fabrication methods, Microelectron. Eng. 159 (2016) 70–74, https://doi.org/10.1016/j.mee.2016.02.063.

[35] A. Krueger, J. Stegk, Y. Liang, L. Lu, G. Jarre, Biotinylated nanodiamond: simple and efficient functionalization of detonation diamond, Langmuir 24 (2008) 4200–4204, https://doi.org/10.1021/la703482v.

[36] Z. Guler, A.S. Sarac, Electrochemical impedance and spectroscopy study of the EDC/NHS activation of the carboxyl groups on poly(ε-caprolactone)/poly(m-anthranilic acid) nanofibers, Express Polym, Lettres 10 (2016) 96–110, https://doi.org/10.3144/expresspolymlett.2016.11.

[37] S. Puertas, P. Batalla, M. Moros, E. Polo, P. del Pino, J.M. Guisan, V. Grazu, J.M. de la Fuente, Taking advantage of unspecific interactions to produce highly active magnetic nanoparticle - antibody conjugates, ACS Nano 5 (2011) 4521–4528, https://doi.org/10.1021/nn200019s.

[38] B. Kalas, J. Nador, E. Agocs, A. Saftics, S. Kurunczi, M. Fried, P. Petrik, Protein adsorption monitored by plasmon-enhanced semi-cylindrical Kretschmann ellipsometry, Appl. Surf. Sci. 421 (2017) 585–592, https://doi.org/10.1016/j.apsusc.2017.04.064.

[39] S.Y. Ong, R.J.J. van Harmelen, N. Norouzi, F. Offens, I.M. Venema, M.B.H. Najafi, R. Schirhagl, Interaction of nanodiamonds with bacteria, Nanoscale 10 (2018) 17117–17124, https://doi.org/10.1039/c8nr05183f.

[40] S. Ghodbane, D. Ballutaud, F. Omnes, C. Agnes, Comparison of the XPS spectra from homoepitaxial {111}, {100} and polycrystalline boron-doped diamond films, Diam. Relat. Mater. 19 (2010) 630–636, https://doi.org/10.1016/j.diamond.2010.01.014.

[41] D. Ballutaud, N. Simon, H. Girard, E. Rzepka, B. Bouchet-Fabre, Photoelectron spectroscopy of hydrogen at the polycrystalline diamond surface, Diam. Relat. Mater. 15 (2006) 716–719, https://doi.org/10.1016/j.diamond.2006.01.004.

[42] J.F. Moulder, W.F. Stickle, P.E. Sobol, Handbook of X-Ray Photoelectron Spectroscopy, Perkin-Elmer, Physical Electronics Division, 1993.

[44] D. Shirley, High-resolution X-ray photoemission spectrum of the valence bands of gold, Phys. Rev. B 5 (1972) 4709–4714.

[45] A.H. Smith, E.M. Robinson, X.Q. Zhang, E.K. Chow, Y. Lin, E. Osawa, J. Xi, D. Ho, Triggered release of therapeutic antibodies from nanodiamond complexes, Nanoscale 3 (2011) 2844–2848, https://doi.org/10.1039/c1nr10278h.

[46] J.M. Say, C. van Vreden, D.J. Reilly, L.J. Brown, J.R. Rabeau, N.J.C. King, Luminescent nanodiamonds for biomedical applications, Biophys. Rev. 3 (2011) 171–184, https://doi.org/10.1007/s12551-011-0056-5.

[47] S.R. Hemelaar, A. Nagl, F. Bigot, M.M. Rodríguez-garcía, M.P. De Vries, M. Chipaux, R. Schirhagl, The interaction of fluorescent nanodiamond probes with cellular media, Microchim. Acta. 184 (2017) 1001–1009, https://doi.org/10.1007/s00604-017-2086-6.

[48] S.Y. Ong, M. Chipaux, A. Nagl, R. Schirhagl, Shape and crystallographic orientation of nanodiamonds for quantum sensing, Phys. Chem. Chem. Phys. 19 (2017) 10748–10752, https://doi.org/10.1039/C6CP07431F.

[49] B. Gottenbos, Antimicrobial effects of positively charged surfaces on adhering Gram-positive and Gram-negative bacteria, J. Antimicrob. Chemother. 48 (2001) 7–13, https://doi.org/10.1093/jac/48.1.7.

[50] J.J.M. Landry, P.T. Pyl, T. Rausch, T. Zichner, M.M. Tekkedil, A.M. Stütz, A. Jauch, R.S. Aiyar, G. Pau, N. Delhomme, J. Gagneur, J.O. Korbel, W. Huber, L.M. Steinmetz, The genomic and transcriptomic landscape of a HeLa cell line, G3.Genes|Genomes|Genetics. 3 (2013) 1213–1224, https://doi.org/10.1534/g3.113.005777.

[51] L. Marchetti, M. Klein, K. Schlett, K. Pfizenmaier, U.L.M. Eisel, Tumor necrosis factor (TNF)-mediated neuroprotection against glutamate-induced excitotoxicity is enhanced by N-methyl-D-aspartate receptor activation: essential role of a TNF receptor 2-mediated phosphatidylinositol 3-kinase-dependent NF-κB pathway, J. Biol. Chem. 279 (2004) 32869–32881, https://doi.org/10.1074/jbc.M311766200.

[52] F. Barry, M.J. Turner, J.M. Schloss, D.R. Glenn, Y. Song, M.D. Lukin, H. Park, R.L. Walsworth, Optical magnetic detection of single-neuron action potentials using quantum defects in diamond, Proc. Natl. Acad. Sci. Unit. States Am. 113 (2016) 14133–14138, https://doi.org/10.1073/pnas.1712523114.

[53] L.T. Hall, G.C.G. Beart, E.A. Thomas, D.A. Simpson, L.P. McGuinness, J.H. Cole, J.H. Manton, R.E. Scholten, F. Jelezko, J. Wrachtrup, S. Petrou, L.C.L. Hollenberg, High spatial and temporal resolution wide-field imaging of neuron activity using quantum NV-diamond, Sci. Rep. 2 (2012) 1–9, https://doi.org/10.1038/srep00401.

[54] D.E.P. Vanpoucke, P. Bultinck, I. Van Driessche, Extending Hirshfeld-I to bulk and periodic materials, J. Comput. Chem. 34 (2013) 405–417, https://doi.org/10.1002/jcc.23088.

[55] D.E.P. Vanpoucke, P. Bultinck, I. Van Driessche, Reply to 'comment on "'Extending Hirshfeld-I to bulk and periodic materials, J. Comput. Chem. 34 (2013) 422–427, https://doi.org/10.1002/jcc.23193.

[56] D.E.P. Vanpoucke, S.S. Nicley, J. Raymakers, W. Maes, K. Haenen, Can europium atoms form luminescent centres in diamond: a combined theoretical–experimental study, Diam. Relat. Mater. 94 (2019) 233–241, https://doi.org/10.1016/j.diamond.2019.02.024.

[57] A. Nagl, S.R. Hemelaar, R. Schirhagl, Improving surface and defect center chemistry of fluorescent nanodiamonds for imaging purposes-a review, Anal. Bioanal. Chem. 407 (2015) 7521–7536, https://doi.org/10.1007/s00216-015-8849-1.

[58] T. Kondo, Y. Niwano, A. Tamura, J. Imai, K. Honda, Y. Einaga, D.A. Tryk, A. Fujishima, T. Kawai, Enhanced electrochemical response in oxidative differential pulse voltammetry of dopamine in the presence of ascorbic acid at

carboxyl-terminated boron-doped diamond electrodes, Electrochim. Acta 54 (2009) 2312–2319, https://doi.org/10.1016/j.electacta.2008.10.073.
[59] S. Stankovich, D.A. Dikin, R.D. Piner, K.A. Kohlhaas, A. Kleinhammes, Y. Jia, Y. Wu, S.B.T. Nguyen, R.S. Ruoff, Synthesis of graphene-based nanosheets via chemical reduction of exfoliated graphite oxide, Carbon N. Y. 45 (2007) 1558–1565, https://doi.org/10.1016/j.carbon.2007.02.034.
[60] C. Wang, N. Huang, H. Zhuang, B. Yang, Z. Zhai, X. Jiang, Photochemical functionalization of diamond films using a short carbon chain acid, Chem. Phys. Lett. 646 (2016) 87–90, https://doi.org/10.1016/j.cplett.2016.01.024.
[61] C. Neeley, Optimizing neuron adhesion and growth by choosing the right surface of Thermo Scientific Chamber Slide, Therm. Sci. (2012) 1–4.